Stabilizing Large-Scale Electric Power Grids with Adaptive Inertia

Julian Fritzsch[1,2,*] and Philippe Jacquod[1,2,†]

[1]*Department of Quantum Matter Physics, University of Geneva, Geneva CH-1211, Switzerland*
[2]*School of Engineering, University of Applied Sciences of Western Switzerland, Haute Ecole Spécialisée de Suisse occidentale (HES-SO), Sion CH-1950, Switzerland*

The stability of ac power grids relies on ancillary services that mitigate frequency fluctuations. The electromechanical inertia of large synchronous generators is currently the only resource to absorb frequency disturbances on subsecond time scales. Replacing standard thermal power plants with inertialess new renewable sources of energy (NREs) therefore jeopardizes grid stability against, e.g., sudden power-generation losses. To guarantee system stability and compensate the lack of electromechanical inertia in grids with large penetrations of NREs, virtual synchronous generators, which emulate conventional generators, have been proposed. Here, we propose a novel control scheme for virtual synchronous generators, where the provided inertia is large at short times—thereby absorbing faults as efficiently as conventional generators—but decreases over a tunable time scale to prevent coherent frequency oscillations from setting in. We evaluate the performance of this adaptive-inertia scheme under sudden power losses in large-scale transmission grids. We find that it systematically outperforms conventional electromechanical inertia and that it is more stable than previously suggested schemes. Numerical simulations show how a quasioptimal geographical distribution of adaptive-inertia devices not only absorbs local faults efficiently but also significantly increases the damping of interarea oscillations. Our results show that the proposed adaptive-inertia control scheme is an excellent solution to strengthen grid stability in future low-inertia power grids with large penetrations of NREs.

I. INTRODUCTION

Alternating-current (ac) power grids are dynamical systems of oscillators—representing rotating generators and frequency-dependent loads—connected to one another by power lines [1,2]. Beyond transporting electricity from producers to consumers, power lines have a dichotomous role. On the one hand, they induce a sufficiently strong coupling to maintain synchrony between oscillators [3,4]—this is necessary for the proper functioning of the system. On the other hand, they propagate frequency waves that may imperil that synchrony [5–11]. Neglecting internal degrees of freedom of generators, the frequency dynamics of ac power grids about their synchronous fixed point are governed by the swing equations [12]. From this set of coupled nonlinear damped wave

equations, it is clear that the electromechanical inertia of conventional power generators based on rotating machines is a very precious resource to absorb disturbances on short subsecond time scales. Simultaneously, inertia favors the long-distance propagation and long-time persistence of subharmonic frequency oscillations [13] which, in the worst instances, lead to grid instability and even blackouts [14]. So far, this dichotomous nature of electromechanical inertia has been dealt with by introducing frequency control—in particular, the so-called droop control—which damps frequency oscillations by adapting the power output of generators to the ac grid frequency [12]. Both inertia and droop control are crucial to the stability of ac power grids and, as of today, both are provided almost exclusively by conventional generators.

The current push toward decarbonization of the energy sector—the largest contributor to global carbon dioxide emissions [15]—induces a strong increase in penetration of new renewable energy sources (NREs) in electric power systems, as fossil-fueled power plants are replaced by wind turbines, photovoltaic panels, and other NREs. The latter differ from traditional power plants in at least three fundamental ways. First, they are volatile and have more fluctuating less predictable power production.

---

*Contact author: julian.fritzsch@etu.unige.ch
†Contact author: philippe.jacquod@gmail.com

Second, they are geographically decentralized. Third, they are connected to the grid via electronic power converters and thus have an altogether different dynamics from standard power plants with electromechanically coupled rotating machines. Increasing the penetration of NREs in power grids therefore implies a significant reduction in the availability of ancillary services such as electromechanical inertia and droop control, with a simultaneous increase in power fluctuations. Because the voltage frequency directly reflects imbalances between power generation and consumption, these power fluctuations result in increased frequency fluctuations [6,9,16–18]. The latter may affect the proper functioning of the grid, as they induce potentially damaging torques on rotating generators, reduce the efficiency of frequency-dependent loads, impact industrial processes that rely on high current quality, or trigger safety devices such as circuit breakers, which operate based on fluctuations of the voltage frequency. Increasing frequency fluctuations while simultaneously reducing resources to mitigate them introduces a number of challenges for grid operators [19].

Various solutions have been proposed to increase the stability of low-inertia grids, one of them being virtual synchronous generators (VSGs) [20,21]. When equipped with electrical-energy storage, VSGs can emulate the response of inertiaful rotating generators by injecting amounts of additional active power proportional to the rate of change of frequency (RoCoF) [22,23]. As they are based on power electronics, the inertia of VSGs is not physical as in conventional generators and can be adapted to the state of the system to improve their performance in, e.g., mitigating frequency fluctuations. Such control schemes go by the name of *adaptive inertia*. In Ref. [24], it is that the droop coefficient of the power-frequency control loop should be varied with the RoCoF, which increases the virtual inertia provided in large RoCoF events. Another adaptive-inertia strategy attempts to minimize the RoCoF and frequency deviation using an on-line optimization of inertia and damping constants [25]. Other control strategies vary both the inertia and the damping proportional to the RoCoF [26]. In Refs. [27,28], a bang-bang control strategy is proposed, focused on a rapid recovery of the synchronized state—a method that, however, displays instabilities [29,30]. Finally, adding a power feedback loop to virtual inertia is proposed in Ref. [31] to keep the RoCoF within predefined bounds.

These investigations have exclusively considered small grids. Accordingly, they have focused on short-time dynamical effects such as the RoCoF and entirely neglected long-range oscillations that adaptive-inertia schemes could generate or help to sustain. Having pointed out above the dichotomous nature of inertia, here we follow an altogether different approach and investigate a novel adaptive-inertia scheme in large-scale power grids. Our approach is tailored to explore regimes of clear

time-scale separation between fast frequency fluctuations and slow coherent oscillations. This approach allows us to differentiate the impact of adaptive inertia on short-distance RoCoF phenomena versus long-range inter-area oscillations [13]. The novel adaptive-inertia control scheme that we propose incorporates a driving force, increasing the inertia at a rate proportional to the absolute value of the RoCoF, and a restoring force bringing the inertia back to its initial low value. The scheme ensures that the inertia (i) increases rapidly in cases of a large RoCoF to quickly mitigate its impact and (ii) decreases quickly once short-time fluctuations have been absorbed, to resynchronize the system quickly and avoid driving long-range oscillations. The performance of this novel adaptive-inertia scheme is assessed against several metrics—frequency- and RoCoF-based l_2^2 norms, the resynchronization time, and the inertial energy supplied to the grid. We find that our adaptive scheme systematically outperforms conventional electromechanical inertia. In particular, it is able to resynchronize the grid at an intermediate frequency value, due to the absence of any dependence on frequency deviation. Finally, numerical results suggest that adaptive-inertia VSGs should, as a matter of priority, be located in peripheral zones.

The paper is organized as follows. In Sec. II, we introduce our model. In Sec. III, we investigate the stability of the extended swing equations. In Sec. IV, we investigate the performance of the extended model on two grids. First, the IEEE RTS-96 grid is used to demonstrate the impact of the different parameters of the driving and restoring force and to visualize the effect of the adaptive inertia. Second, we use a model of the European high-voltage power grid to investigate the effect of the adaptive inertia on a strongly connected large-scale grid. We emphasize that the impact of the adaptive inertia on the performance is largest when it is located in peripheral areas. Conclusions and final discussions are given in Sec. V.

II. THE MODEL AND THE ADAPTIVE-INERTIA CONTROL SCHEME

The state of an ac power grid is determined by voltage angles and amplitudes at all of its nodes. At steady state, these cooordinates are determined by power-flow equations, which combine Ohm's and Kirchhoff's laws [1,12]. A perturbation such as a sudden line opening by a circuit breaker, or a rapid disconnection of a large generator or load, induces transient voltage dynamics. Under the standard assumption that there is a time-scale separation in the dynamics of the voltage angle versus its amplitude, and focusing on time scales from subseconds to a few tens of seconds, that voltage amplitudes can be considered constant and one can focus on the voltage-angle dynamics. These dynamics are different at generator and load nodes. Voltage angles at generator nodes are governed by

the so-called swing equations. In the lossless line approximation—justified for high-voltage grids—the equation for generator i reads [1,12]

$$m_i \dot{\omega}_i + d_i \omega_i = P_i - \sum_j b_{ij} \sin(\theta_i - \theta_j), \qquad (1)$$

where m_i is the inertia of the ith generator, d_i is its damping parameter, θ_i is its voltage angle, $\omega_i = \dot{\theta}_i$ is the deviation of its angular frequency from the rated frequency, and $P_i > 0$ is the generated power. Finally, nodes are coupled by lines with susceptances $\tilde{b}_{ij}$ and $b_{ij} = \tilde{b}_{ij} V_i V_j$ is the product of that susceptance with the voltage magnitudes (assumed constant) at nodes i and j. Renewable energy sources are inertialess and are modeled as

$$d_i \omega_i = P_i - \sum_j b_{ij} \sin(\theta_i - \theta_j). \qquad (2)$$

We use the structure-preserving model [32], according to which the voltage-angle dynamics at loads are also described by Eq. (2), where d_i now gives the frequency dependence of the load and $P_i < 0$ is the consumed power.

If all nodes had inertia, the dynamics of voltage angles would be determined by a discrete nonlinear damped wave equation, as in Eq. (1). In real power grids, typically one node out of ten is a generator node; therefore, the wave dynamics are superimposed on a background diffusion equation [see Eq. (2)]. The frequency-dependence constant d_i is, however, very small for loads, resulting in a large diffusion constant and, accordingly, a quasiballistic propagation of voltage-angle waves between generator nodes.

Equations (1) and (2) give the dynamics in a power grid with conventional and NRE generators. When, additionally, one has a VSG with adaptive inertia—say, at node i—Eq. (1) is augmented by

$$\dot{m}_i = \alpha_i |\dot{\omega}_i| - \beta_i (m_i - m_{\min,i}), \qquad (3)$$

which defines our novel adaptive-inertia scheme. It assumes that there is a minimal amount $m_{\min,i} > 0$ of inertia present at all times. Two control parameters further determine the dynamical evolution $m_i(t)$ as a frequency disturbance $\dot{\omega}_i \neq 0$ hits node i. First, the gain $\alpha_i > 0$ controls the short-time increase and the maximum amount of inertia to absorb that disturbance. Second, $\beta_i > 0$ models a restoring force and controls the rate at which inertia returns to its minimal amount, in order to minimize its contribution to the further propagation of frequency disturbances. A block diagram of the proposed control scheme [see Eq. (3)] is shown in Fig. 1. An important feature of our adaptive-inertia scheme is that because it depends only on the frequency derivative—the RoCoF—and not on the frequency itself, it is able to synchronize at an intermediate frequency value unlike, e.g., the bang-bang scheme,
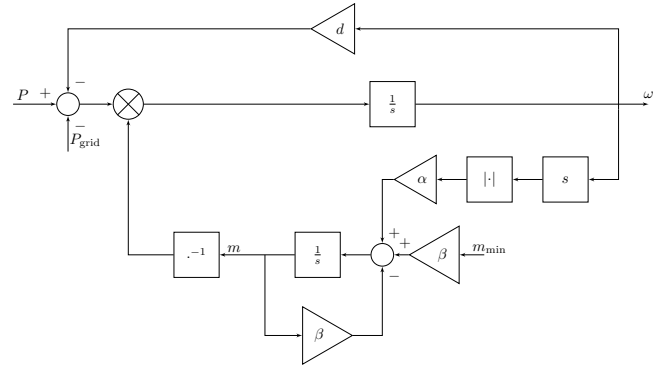

FIG. 1. The block diagram of our proposed adaptive-inertia scheme. P_{grid} is the power flow across the lines connected to the generator. It is given by the sine terms of the power-flow equation [Eq. (1)].

which explicitly depends on the frequency. The two control parameters, α_i and β_i, need to be tuned to optimally absorb large RoCoF values and to make the system return quickly to the steady state. In Sec. S1 of the Supplemental Material [33], we give an illustrative example that demonstrates the action of our adaptive-inertia method on a single-machine infinite-bus model.

III. STABILITY OF THE CONTROL SCHEME

Previously proposed adaptive-inertia schemes generate instabilities in certain circumstances [29,30] and we first show that our scheme does not introduce any such instability. Equation (3) cannot be linearized about the synchronous state, as the derivative of $|\dot{\omega}|$ is not defined at $\dot{\omega} = 0$. We therefore introduce a small dead band $\varepsilon \geq 0$ into Eq. (3) without changing the fixed point,

$$\dot{m}_i = \frac{1}{2}\alpha_i (|\dot{\omega}_i + \varepsilon| + |\dot{\omega}_i - \varepsilon|) - \beta_i (m_i - m_{\min,i}) - \alpha_i \varepsilon, \qquad (4)$$

where $0 < \varepsilon \ll 1$. For $\varepsilon \to 0$, we recover the original Eq. (3). This mathematical trick allows us to linearize Eqs. (1)–(3) about a fixed point with $\omega_i = \delta\omega$, $\theta_i = \theta_i^0 + \delta\theta_i$, $m_i = m_{\min,i} + \delta m_i$, and $P = P_i^0 + \delta P_i$. Without loss of generality, we assume that there are only generator nodes with adaptive inertia. The linearized equations then read

$$\begin{bmatrix} \delta\dot{\boldsymbol{\theta}} \\ \delta\dot{\boldsymbol{\omega}} \\ \delta\dot{\boldsymbol{m}} \end{bmatrix} = \begin{bmatrix} \mathbf{0} & \mathbf{1} & \mathbf{0} \\ -\mathbf{M}_m^{-1}\mathbf{L} & -\mathbf{M}_m^{-1}\mathbf{D} & \mathbf{0} \\ \mathbf{0} & \mathbf{0} & -\boldsymbol{\beta} \end{bmatrix} \begin{bmatrix} \delta\boldsymbol{\theta} \\ \delta\boldsymbol{\omega} \\ \delta\boldsymbol{m} \end{bmatrix} + \begin{bmatrix} \mathbf{0} \\ \delta\boldsymbol{P} \\ \mathbf{0} \end{bmatrix}, \qquad (5)$$

where $\delta\boldsymbol{\theta} = (\delta\theta_1, \dots)$, $\delta\boldsymbol{\omega} = (\delta\omega_1, \dots)$, $\delta\boldsymbol{m} = (\delta m_1, \dots)$, $\delta\boldsymbol{P} = (\delta P_1, \dots)$, $\mathbf{M}_m = \mathrm{diag}(m_{\min,i})$, $\mathbf{D} = \mathrm{diag}(d_i)$,

$\boldsymbol{\beta} = \text{diag}(\beta_i)$, and $\mathbf{L}$ is the network Laplacian, defined as

$$\mathbf{L}_{ij} = \begin{cases} -b_{ij}\cos(\theta_i^0 - \theta_j^0), & \text{for } i \neq j, \\ \sum_k b_{ik}\cos(\theta_i^0 - \theta_k^0), & \text{for } i = j. \end{cases} \quad (6)$$

The stability matrix in Eq. (5) is negative semidefinite because (i) its sub-block

$$\mathbf{A} = \begin{bmatrix} \mathbf{0} & \mathbf{1} \\ -\mathbf{M}_m^{-1}\mathbf{L} & -\mathbf{M}_m^{-1}\mathbf{D} \end{bmatrix} \quad (7)$$

is the stability matrix of a system with conventional generators with inertia $m_{\text{min},i}$ and (ii) the restoring parameters $\beta_i > 0$. This guarantees the linear stability of our adaptive-inertia control scheme.

IV. NUMERICAL SIMULATIONS

We evaluate the efficiency of our adaptive-inertia control scheme by investigating the frequency response following a step change in the active power injected by a generator. We consider both step changes in the production of conventional generators and of VSGs. We measure the grid response against four different performance measures, chosen to be sensitive to various dynamical aspects. We consider l_2^2 norms of the frequency and of the RoCoF:

$$l_2^2(\omega) = \sum_i \int_0^\infty (\omega_i(t) - \omega_{\text{sync}})^2 dt, \quad (8)$$

$$l_2^2(\dot{\omega}) = \sum_i \int_0^\infty \dot{\omega}_i(t)^2 dt \quad (9)$$

and the energy injected into the grid by the inertial response,

$$E_{\text{rot}} = -\sum_i \int_0^\infty m_i(t)\dot{\omega}_i(t) dt, \quad (10)$$

as well as the resynchronization time t_{re}. We define the latter as the time it takes to damp frequency deviations down to less than $1\,\text{mHz}$ on all nodes. These four performance measures are sensitive to various dynamical features—from short-time rapid frequency disturbances to long-time large-scale coherent interarea oscillations. Optimizing our adaptive-inertia scheme with respect to all of these—which is feasible, as we find below—guarantees an overall quasioptimal disturbance-mitigation protocol.

Before presenting numerical results, we qualitatively discuss the influence of the control parameters α_i and β_i on the performance measures. Equation (3) makes it clear that the large RoCoF following a fault increases the inertia until the RoCoF is sufficiently small or the inertia sufficiently large that the second term on its right-hand side

dominates and relaxes the inertia back to its minimal value. The short-time behavior is therefore dominantly impacted by α_i and the long-term behavior by β_i. Next, the frequency performance measure, given in Eq. (8), is strongly influenced by long-lived sustained frequency oscillations, while the RoCoF performance measure, given in Eq. (9), is mostly determined by the short-time dynamics directly following the fault. Finally, the resynchronization time is, by definition, linked to the long time system dynamics. Putting all this together, we expect the frequency and the resynchronization-time performance measures to improve with increasing β_i, whereas the RoCoF performance measure should improve with α_i. We furthermore expect that the injected energy performance measure, given in Eq. (10), depends nontrivially on both α_i and β_i, as it explicitly depends on both the RoCoF and the inertia. The response of the system is stronger when the size ΔP of the fault increases. We further expect a scaling behavior where the response remains the same when

$$\frac{\alpha_i}{\Delta P_i} = \text{const.} \quad (11)$$

This follows from the fact that the RoCoF is given by [12]

$$\dot{\omega}_i(t = 0) = \frac{\Delta P_i}{m_i} \quad (12)$$

together with Eq. (3). This scaling is confirmed in Fig. 4.

We next compare the performance measures for networks with and without VSGs. The networks considered are the IEEE RTS-96 network [34] and *PanTaGruEl*, a model of the synchronous grid of continental Europe [7,35].

A. IEEE RTS-96

We begin by investigating the IEEE RTS-96 test case shown in Fig. 2. It is partitioned into three areas with ten generation units each. The remaining nodes are loads. In the default case, all of the generation units are conventional generators. For evaluation of our method, we promote two of the generation units in each area to VSGs equipped with the adaptive-inertia method [see Eq. (3)]. Following the standard of power systems, all physical quantities are expressed in the *per unit system*, which is obtained by division with some common base unit [12]. Static physical quantities such as line capacities and power injections and consumptions are defined in Ref. [34]. The inertia of conventional generators is randomly drawn from a uniform distribution, $m_i \in [0.1\,\text{PU}, 1, 1\,\text{PU}]$ and each damping corresponds to a fixed ratio $d_i/m_i \approx 0.3$. The chosen inertia range is typical for generators with a maximum production of the order of $100\,\text{MW}$ to $1\,\text{GW}$. For the adaptive generators, the initial inertia m_{min} is set to one third of the randomly drawn inertia in the default case. Other parameters are the same for all VSGs. The fault considered is
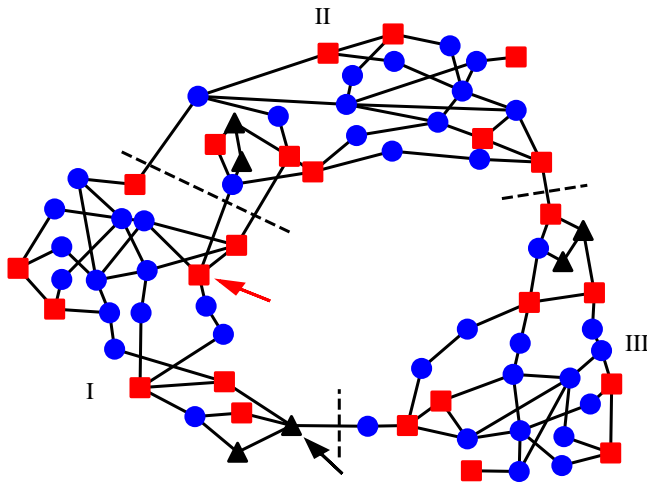
FIG. 2. The IEEE RTS-96 network. The red squares are conventional generators, the black triangles are VSGs equipped with the adaptive-inertia method [see Eq. (3)], and the blue circles are load nodes. The black arrow indicates the VSG where the power is varied and the red arrow indicates the conventional generator at which a fault is applied. The roman numerals label the different areas and the dashed lines indicate their boundaries.

FIG. 3. The dependence of (a) the frequency performance measure $l_2^2(\omega)$ [see Eq. (8)], (b) the RoCoF performance measure $l_2^2(\dot\omega)$ [see Eq. (9)], (c) the injected inertial energy E_{rot} [see Eq. (10)], and (d) the resynchronization time, t_{re}, on the VSG control parameters α and β defined in Eq. (3). The fault considered is a change in the power at the generator, indicated by the black arrow in Fig. 2. The ratios of the performance measures with VSGs compared to those with only conventional generation are color coded. The blue-colored areas correspond to the adaptive method performing better than conventional generators.

an instantaneous 25% reduction of the power generated by the VSG with adaptive inertia, marked by a black arrow in Fig. 2. In Fig. 3, we show the ratio of each of the four performance measures with and without VSGs. Figures 3(a), 3(b), and Fig. 3(d) confirm our above expectations that the frequency performance measure and the resynchronization time improve with β, while the RoCoF performance measure improves with α. Figure 3(b) further shows that $l_2^2(\dot\omega)$ has a weak dependence on β, which is only visible at small β, when generator oscillations following a fault persist longer. Next, the data in Fig. 3(a) depend on the ratio α/β and not individually on α or β. We find that this is the case because fixing α/β gives similar time profiles for $m(t)$, with, in particular, a similar maximal inertia value. Increasing α and β while keeping their ratio fixed gives a faster rise of virtual inertia, which does not affect the long-time dynamics. It therefore leaves $l_2^2(\omega)$ mostly unchanged. It is remarkable that the injected-energy performance measure, shown in Fig. 3(c), exhibits the same behavior as $l_2^2(\omega)$. This suggests that it is dominated by long-term dynamical effects. Finally, the resynchronization time exhibits a more intricate behavior, with an optimal performance at large α and medium β instead of $\beta \gg \alpha$ as expected. We find that this behavior, however, depends on the fault location and even more on the network considered. In Fig. 4, we show the validity of the scaling, given in Eq. (11). The three subplots look the same when the horizontal axis is scaled with the size of the fault. Additionally, we find, but do not show, that the performance improves with the number of VSGs in the grid. Overall, the best global performance is obtained for both $\alpha, \beta \gg 1$.
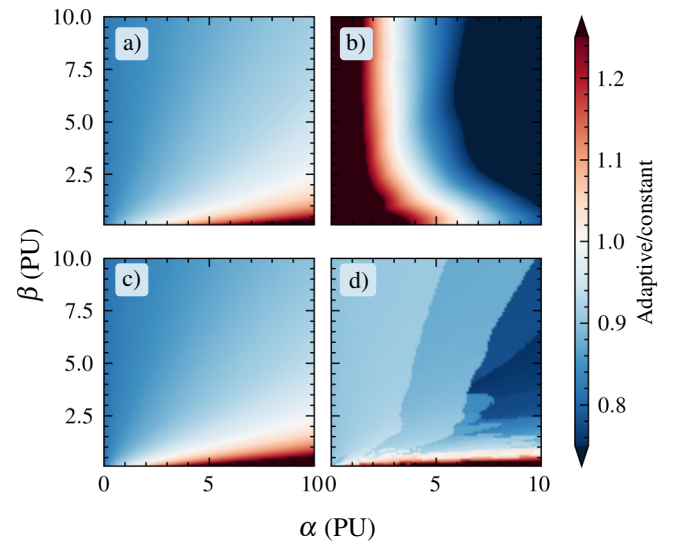
Finally, we point out that the performance improves with the number of VSGs in the grid.

In the following, we investigate dynamical effects in some more detail for $\alpha = \beta = 5\,\text{PU}$. In Fig. 5, we illustrate the dynamics of the faulted generator, for the constant-inertia case (black curve) and the case with homogeneous VSGs with $\alpha = \beta = 5\,\text{PU}$ (red curve). To better connect with ac power engineering, we plot the voltage frequency, $f = \omega/2\pi$ and frequency RoCoF, $\dot f = \dot\omega/2\pi$. First, the amplitude of oscillations of the frequency, as well as their short-period components, are significantly reduced by the adaptive-inertia method. This is directly reflected in the frequency performance measure and in a reduced resynchronization time, $t_{\text{re,adapt}} = 16.3\,\text{s} < t_{\text{re,const}} = 18.5\,\text{s}$. Second, the adaptive inertia also improves the RoCoF performance measure significantly, as it quickly leads to smaller slower oscillations of $\dot f$. Furthermore, once $\dot f$ has decreased sufficiently, the lower inertia leads to even fewer oscillations and a rapid recovery of the system in the adaptive scheme. There is a large initial RoCoF when the faulted generator is a VSG. This is expected, as the RoCoF is inversely proportional to the inertia right after the fault [see Eq. (12)] and the initial inertia m_{min} in the adaptive case has been chosen at one third of its value in the constant-inertia case.
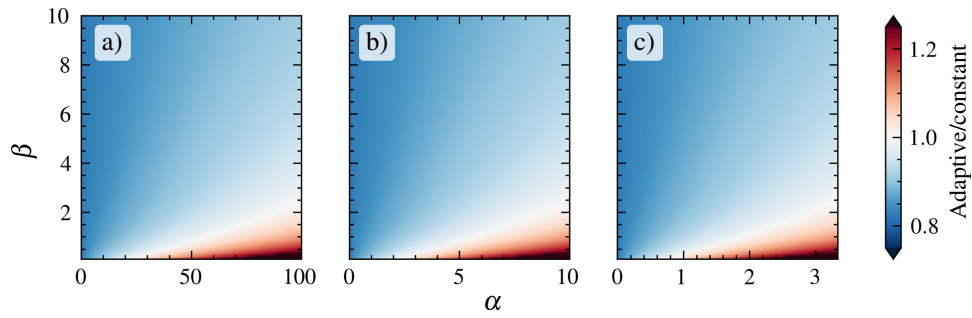
FIG. 4. The frequency performance measure, given in Eq. (8), for a fault of size (a) $\Delta P = -0.1 \, \mathrm{PU}$, (b) $\Delta P = -1.0 \, \mathrm{PU}$, and (c) $\Delta P = -3.0 \, \mathrm{PU}$ on the VSG marked by a black arrow in Fig. 2. The ratios of the performance measures with VSGs compared to those with only conventional generation are color coded. The blue-colored areas correspond to the adaptive method performing better than conventional generators.

That feature affects only the dynamics of the faulted generator and is not a problem as long as the latter functions purely on power electronics. However, in cases in which $m_{\min}$ is provided by physical electromechanically coupled inertia, or if the VSG is connected to the same bus as some conventional generation, this large initial RoCoF needs to be mitigated. This can be achieved by resetting the inertia to a larger value $m(t \leq 0) > m_{\min}$ once the frequency stays within some predefined range over a period of time (e.g.,
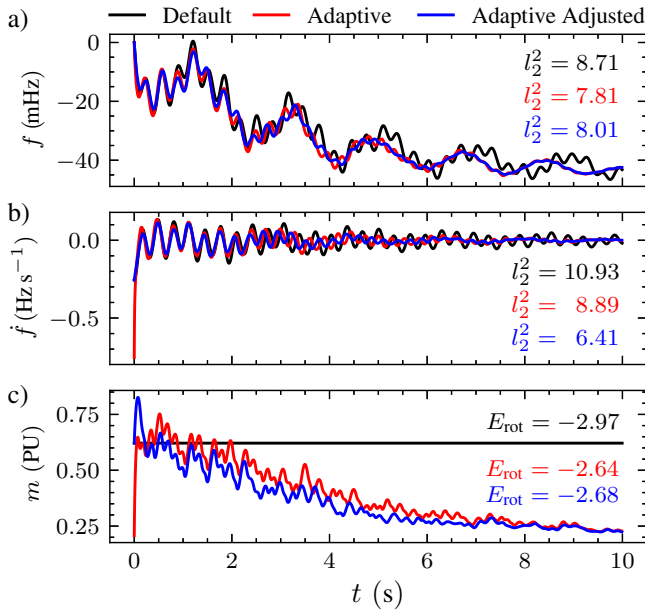

FIG. 5. The time evolution of (a) the frequency, $f = \omega/2\pi$, (b) the RoCoF, $\dot{f} = \dot{\omega}/2\pi$, and (c) the inertia following a change of $\delta P = -1 \, \mathrm{PU}$ at the VSG indicated by the black arrow in Fig. 2. The black line corresponds to the default case with only conventional generation. The red line corresponds to the scenario with six generators being equipped with our adaptive method. The blue line corresponds to the adaptive scenario adjusted with an initial inertia of the VSGs set to the value of the default case.

it does not deviate by more than $0.05 \, \mathrm{Hz}$ from the synchronized state for 1 min). This adjusted adapted-inertia scheme adds the benefit of greatly decreasing the initial RoCoF while not losing the advantage of the decaying inertia. In our case, setting $m_{i,\mathrm{adapt.}}(t = 0) = m_{i,\mathrm{const}}$ leads to a small penalty on the frequency performance measure and the energy injected while more than halving the maximum RoCoF and decreasing the RoCoF performance measure significantly (blue curves in Fig. 5). In Fig. 5, we finally show the time evolution of the inertia of the faulted generator. With the adaptive scheme, the inertia shoots up right after the fault and then decays back to its minimal value.

We conclude that for sufficiently large control parameters α and β, our adaptive-inertia control scheme outperforms the constant-inertia method for all four performance measures. In Figs. 3 and 5, we make it clear that this occurs because VSGs perform equally as well as conventional inertial generators at absorbing the short-time RoCoF but damp frequency oscillations more quickly. A closer look at how this is done in practice reveals an interesting dual action, in which VSGs simultaneously fight inter- and intra-area oscillations. In Fig. 6(a), it is shown that areas I and II (see Fig. 2) oscillate against each other—the fault has triggered an interarea oscillation mode. We find that these modes are more efficiently damped by VSGs than by conventional generators. Furthermore, VSGs equipped with our adaptive-inertia control scheme lead to a more homogeneous response and an enhanced intra-area coherency. The effect is quantified by the coherency measure

$$l_2^2(\mathrm{coh}) = \sum_i \int_0^\infty (\omega_i(t) - \bar{\omega}_{\mathrm{area}}(t))^2 \, dt, \quad (13)$$

where $\bar{\omega}_{\mathrm{area}}(t)$ is the mean frequency in the area corresponding to node i. In Fig. 6(b), it is shown that the integrand of Eq. (13) decays exponentially faster with than without VSGs. Due to VSGs, all generators within one area
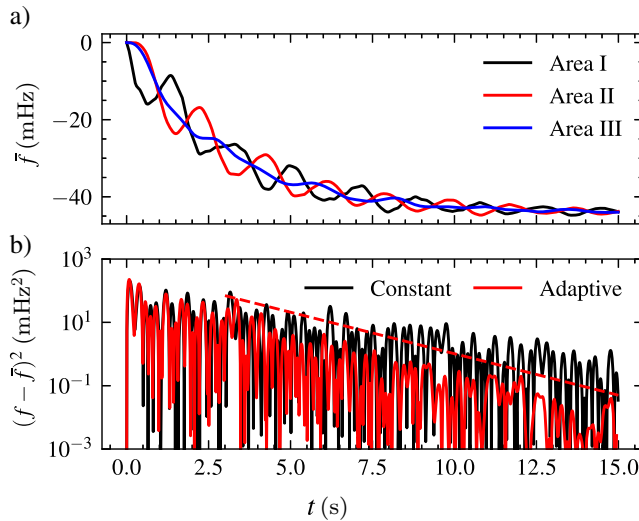
FIG. 6. (a) The time evolution of the average frequency $\bar{f}$ in each of the three areas of the RTS96 model of Fig. 2. Interarea oscillations between areas I and II can clearly be seen. (b) The time evolution of the frequency variance around $\bar{f}$ in each area. The coherency of each area is enhanced in the presence of VSGs with adaptive inertia (red curve), with an exponential reduction of $(f - \bar{f})^2$ (dashed red line).

quickly respond coherently, with their frequency oscillating closer and closer to the area average shown in Fig. 6(a). We find that the coherence measure for the adaptive case is only 75% of the measure for the constant case. A very interesting finding is therefore that the adaptive-inertia scheme of Eq. (3) damps not only interarea oscillations but also intra-area machine-machine oscillations.

Finally, we find that the situation is similar for a fault on one of the conventional generators. For a fault on the generator marked by the red arrow in Fig. 2, we find that the results for the frequency performance measure as well as the energy and resynchronization time closely resemble panels Fig. 3(a), 3(c), and 3(d). The adaptive case also performs better than the conventional inertia case. For the RoCoF performance measure, however, the improvement is significantly smaller than the one shown in Fig. 3. This is not surprising when the fault is some distance away from the nearest VSG, since the RoCoF is mostly determined by local short-time dynamics. These results are shown in Sec. S2 of the Supplemental Material [33].

B. PanTaGruEl model of the synchronous grid of continental Europe

Large-scale power-grid models have a clearer time-scale separation and accordingly enable better evaluations of the performance of our adaptive-inertia control scheme. Therefore, we now turn our attention to a continental-size transmission grid. PanTaGruEl is a model of the synchronous transmission grid of continental Europe. It
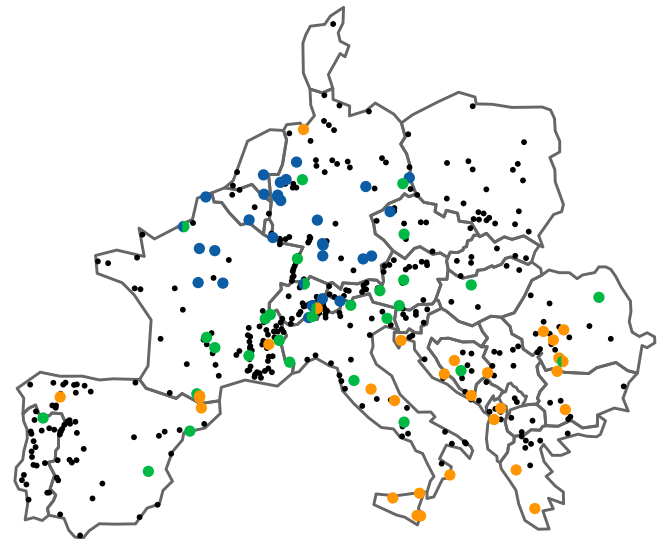

FIG. 7. The PanTaGruEl model of the synchronous grid of continental Europe. The dots indicate the geographical locations of power generators. The black dots correspond to generators that are always conventional machines with electromechanical inertia. The colored dots correspond to VSGs with adaptive inertia in configurations corresponding to central distribution (blue), peripheral distribution (orange), and homogeneous distribution (green) of VSGs and to conventional generators otherwise. All of the colored dots are VSGs in the configuration corresponding to the total distribution.

consists of 3809 nodes and 7343 lines, encompassing all lines at voltages of 200 kV and above [7,35]. We use a generation dispatch where 448 nodes are generators and promote some of those generators to VSGs with adaptive inertia. We choose how the VSGs are located following three different distributions where 30 VSGs are located centrally, peripherally, or homogeneously, according to the resistance-distance centrality [35,36]. Details of how this is done are discussed below. We further consider a distribution including all 86 different VSGs from these three distributions (four VSGs are included in both the homogeneous and either the central or the peripheral distribution). In Fig. 7, we show the location of the VSGs and of the conventional generators for each of these distributions.

The minimum inertia $m_{\mathrm{min},i}$ of the VSGs is set at one third of their original constant inertia. We choose $\alpha = \beta = 10\,\mathrm{PU}$ which according to Fig. 3 is expected to give excellent performance. This is confirmed in Fig. 8 for the PanTaGruEl model, where we show a parameter sweep similar to the one in Sec. IV A for a 100-mW fault on a VSG in Switzerland. In Sec. IV A, we have focused on the effect of our adaptive method when the power change occurs at one VSG. In this section, we want to investigate the effect on the overall stability of the grid when a fault occurs at a conventional generator. This is motivated by the much larger scale of PanTaGruEl compared to the RTS-96
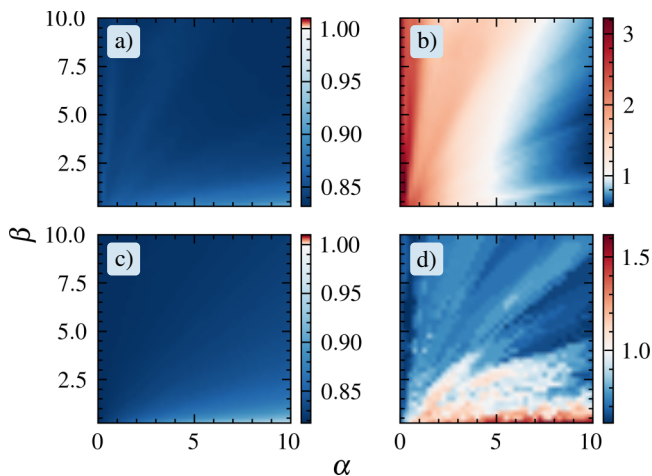
FIG. 8. The dependence of (a) the frequency performance measure $l_2^2(\omega)$ [Eq. (8)], (b) the RoCoF performance measure $l_2^2(\dot{\omega})$ [Eq. (9)], (c) the injected inertial energy $E_{\rm rot}$ [Eq. (10)], and (d) the resynchronization time, $t_{\rm re}$, on the VSG control parameters α and β defined in Eq. (3). The fault considered is a 100-mW power loss at a VSG in Switzerland. The ratios of the performance measures with VSGs compared to those with only conventional generation are color coded. The blue-colored areas correspond to the adaptive method performing better than conventional generators.
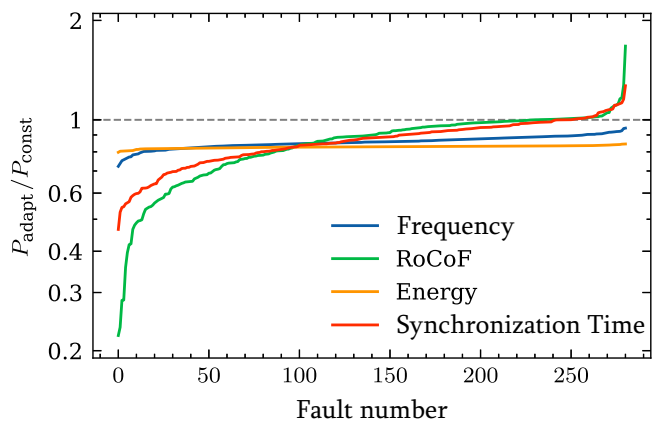

FIG. 9. The ratio of the performance measures with constant inertia only versus those with adaptive inertia on 86 VSGs located on the colored dots in Fig. 7, on a log scale. The values below the dashed line correspond to our adaptive scheme performing better and the values above correspond to the default case, with only constant inertia performing better. To improve readability, the faults are ordered independently for each curve to make the latter monotonically increasing.

grid and the fact that for practical financial reasons, only a minority of generators can be promoted to VSGs in a real large-scale power grid. Of particular interest is to determine if the significantly improved network performance discussed in Sec. IV A persist when the distance between faulted generation and VSGs grows.

1. Total distribution of adaptive inertia

We simulate instantaneous power losses of 100 MW on each of the 281 conventional generators with $P_i^0 \geq 100$ MW (there are 81 generators that produce less than 100 MW in the used dispatch) and first compare the conventional inertia case to a grid with a distribution of VSGs on all 86 colored nodes in Fig. 7. In Fig. 9, we show the ratio of the four performance measures with and without adaptive-inertia VSGs, for the 281 individual faults. Our adaptive-inertia scheme clearly almost always outperforms the constant-inertia case: the frequency performance improves in all cases, while approximately 17% less energy is needed to stabilize the grid. Resynchronization occurs faster for 88% of the faults considered. The situation is less clear when considering the RoCoF performance measure of Eq. (9), which varies by over 3 orders of magnitude. This is so because the RoCoF is a local measure: faults on weakly connected generators with low inertia give rise to much larger RoCoF values compared to faults on large power plants in very densely connected

areas. In 82% of all cases, the RoCoF performance measure improves with adaptive inertia. Generally, it does not improve when the faulted generator lies in a central well-connected area with a high density of inertial generators, where RoCoFs are small to start with. For instance, the two worst cases where the performance measure decreases by more than 20% correspond to faults the RoCoF responses of which are among the seven smallest ones, out of the 281 considered faults. We conclude that our adaptive-inertia control scheme significantly improves grid performance for all faults that may be problematic in the constant-inertia case.

2. Geographical distribution of adaptive inertia

Previous work has shown that geographically homogeneous distributions of conventional inertia optimize the grid response against frequency disturbances [37,38] and a practical question that naturally arises is where financially limited resources of adaptive inertia should, as a matter of priority, be located. The fact that VSGs do not improve the RoCoF performance for central faults suggests that the performance is better when VSGs are distributed in peripheral regions that support interarea oscillations [13,39] and where disturbances are larger to start with [35]. To test this hypothesis, we compare the performance for three different distributions of 30 VSGs. The first two have VSGs distributed either centrally or peripherally. They are obtained by picking every other generator out of the 60 most or least central ones, respectively, according to their average resistance-distance centrality [36]. The third one considers 30 VSGs homogeneously distributed in terms of their centrality. The location of the VSGs in each case is shown in
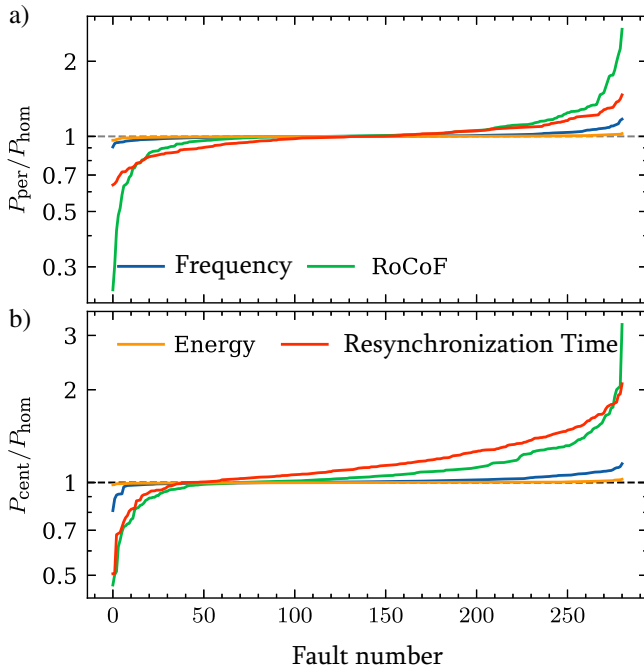
FIG. 10. The ratio of the performance measures for 30 VSGs distributed in (a) the peripheral and (b) the central parts of the grid with those obtained for a homogeneous distribution of VSGs (see the discussion in the text and Fig. 7). In (a), the values below the dashed line correspond to the peripheral distribution performing better and the values above correspond to the homogeneous distribution performing better. Similarly, in (b), the values below the dashed line correspond to the central distribution performing better and the values above correspond to the homogeneous distribution performing better. To improve readability, the faults are ordered independently for each curve to make the latter monotonically increasing.

Fig. 7. To ensure legitimate comparisons, we have fixed the total minimum amount of inertia in the grid at the same value in all cases.

The results are presented in Fig. 10. First, we can clearly see that the central distribution worsens the grid response according to all performance measures, in almost all fault cases, especially from the point of view of the RoCoF and resynchronization performance measures. Second, we find that, overall, peripheral and homogeneous geographical distributions of VSGs perform similarly, according to the frequency, the energy, and the resynchronization-time performance measures. Third, the peripheral distribution of VSGs improves the RoCoF performance measure in the majority of fault cases over the homogeneous distribution. Furthermore, we find that in almost all instances where the peripheral distribution gives a worse RoCoF response than the homogeneous distribution, the RoCoF response itself is small, so that the worsened response is unproblematic.

Our results therefore indicate that both homogeneous and peripheral distributions of VSGs are viable options,
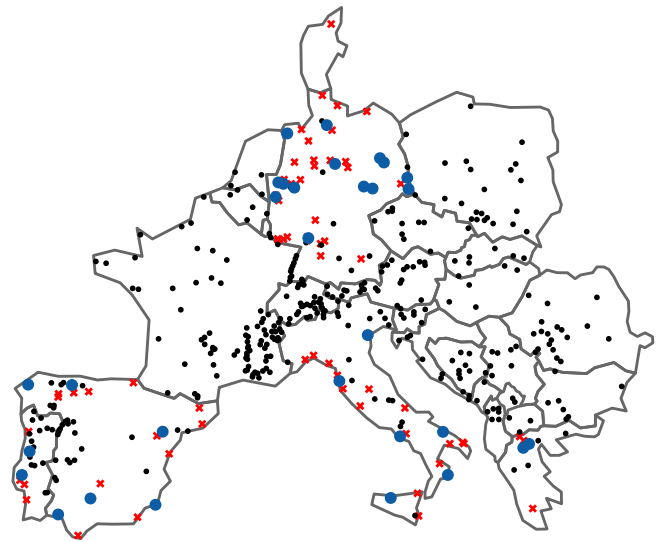

FIG. 11. The locations of the machines with adaptive inertia (blue dots) and the conventional machines (black dots) for a future scenario in which generators powered by fossil fuels have been replaced with renewable (inertialess) generation. The generators that are turned into renewable generation and not replaced with VSGs are shown by red crosses. Note the reduced density of generators in Portugal, Spain, Italy, Greece, Germany, and Denmark.

with a slight, but not too significant, advantage for the peripheral distribution. Interestingly, the latter significantly outperforms all other distributions when the fault is located in the Balkans or the Iberian Peninsula. These are the areas supporting the modes driving the east-west inter-area oscillations [39], which corroborate the hypothesis made in the previous paragraph, that the adaptive-inertia control scheme also improves the damping of interarea oscillations.

3. Future scenario with reduced electromechanical inertia

We finally investigate a future scenario of a well-developed energy transition, in which the penetration of renewable energy sources has been significantly increased. Accordingly, we turn all the fossil-fuel generators in Greece, Italy, Germany, Denmark, and the Iberian Peninsula into renewable generators of the same rated power, i.e., by turning their dynamics from Eq. (1) to Eq. (2), while keeping the damping parameter the same. This corresponds to droop-controlled inverters providing frequency control [40]. In total, 94 generators are changed, corresponding to a total inertia reduction by 31 %. They are indicated by red crosses in Fig. 11.

To investigate whether adaptive inertia can compensate for the inertia reduction, we consider three different distributions of VSGs. First and second, we consider VSGs on the peripheral and homogeneous distributions,
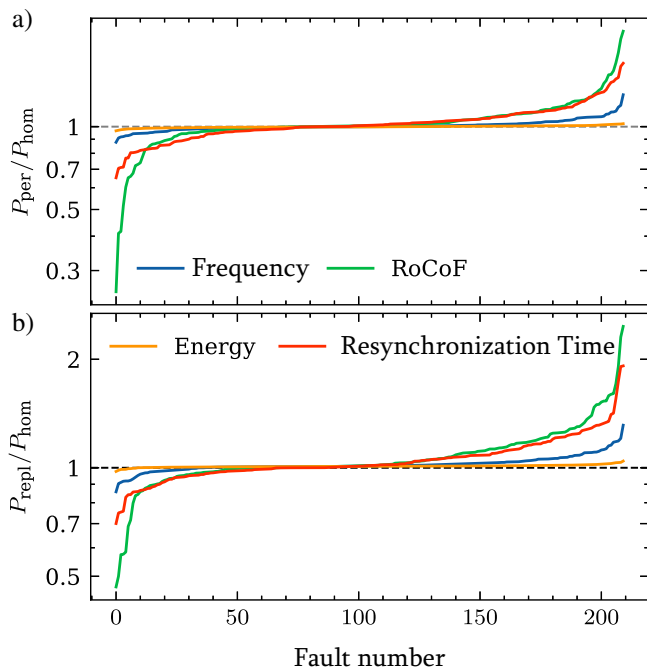
FIG. 12.   The ratio of the performance measures for 30 VSGs distributed in (a) the peripheral part of the grid and over (b) removed conventional generators, with those obtained for a homogeneous distribution for the new renewables scenario. The values below the dashed line correspond to our adaptive scheme performing better and the values above correspond to the default case with only constant inertia performing better. To improve readability, the faults are ordered independently for each curve, to make the latter monotonically increasing.
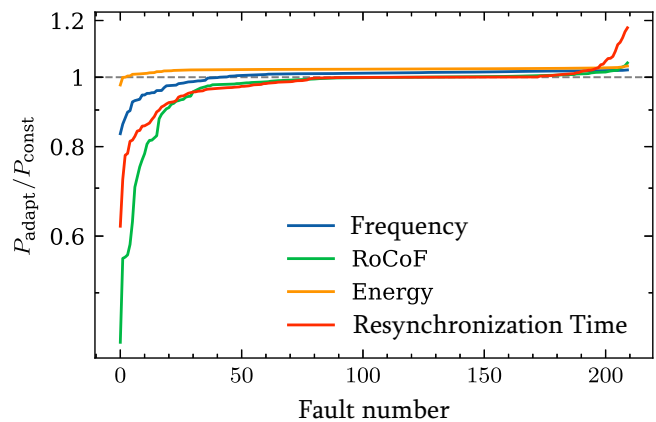

FIG. 13.   The ratio of the performance measures for 30 VSGs distributed over the removed conventional generators to those of the case without VSGs for the new renewables scenario. The values below the dashed line correspond to our adaptive scheme performing better and the values above correspond to the default case with only constant inertia performing better. To improve readability, the faults are ordered independently for each curve to make the latter monotonically increasing.

respectively, the excellent performance of which has been emphasized in Sec. IV B 2. We further take account of the fact that rotating machines can be converted into synthetic inertia as power electronic controlled synchronous condensers. Accordingly, we consider a third distribution in which 30 of the fossil-fuel generators turned renewable generators are promoted to VSGs with adaptive inertia. This new distribution of inertial generation is shown in Fig. 11. To ensure that the minimum amount of inertia is the same in all three cases, we set the minimum inertia to 10% of the inertia of the former conventional generation for the VSGs installed at renewable buses and to 110% of the constant inertia for VSGs installed at buses with conventional generation.

The results are shown in Figs. 12 and 13. Figure 12 confirms the results of Sec. IV B 2: the peripheral distribution of VSGs has a slight, though still significant, advantage over the homogenous one. They both perform better than the case in which VSGs are distributed over fossil-fuel generators turned renewables. We stress that this latter distribution still contains buses over a large range of centralities. Nevertheless, this latter distribution performs significantly better than turning fossil-fuel generators into

renewables without inertia compensation, as is clearly shown in Fig. 13. There are very few faults for which the resynchronization time increases a little, which, however, correspond to the shortest resynchronization times. We conclude that VSGs with our adaptive-inertia schemes are solutions of choice to support grid stability upon increasing the penetration of renewable generation.

V. CONCLUSIONS

Decarbonization of the energy sector requires a strong increase in the penetration of new renewable sources of energy. This increase will be accompanied by a significant reduction of available electromechanical inertia. Therefore, guaranteeing the dynamical stability of future electric power grids is one of the main challenges facing the energy transition. Motivated by the ambivalent nature of inertia, which absorbs frequency disturbances at short times but helps them propagate at later times, we propose to deploy virtual synchronous generators controlled by an innovative adaptive-inertia scheme, given in Eq. (3), to guarantee the stability of future power grids. Unlike previously proposed virtual-inertia schemes, ours is always stable. Moreover, it outperforms the electromechanical inertia from conventional generators for both short- and long-time effects, essentially regardless of the location of the considered fault. In fact, our scheme not only absorbs strong frequency disturbances at short time scales but, moreover, it efficiently damps long-range long-time interarea oscillations. While the evidence suggests that VSGs with adaptive inertia should, as a matter of priority, be located in peripheral

areas, distributing them homogeneously or where fossil-fueled generators have been replaced by NREs also significantly enhances grid stability. VSGs controlled with the proposed adaptive-inertia scheme should therefore be considered as serious candidates to help stabilize future decarbonized power grids.

ACKNOWLEDGMENTS

[1] A. R. Bergen and V. Vittal, *Power Systems Analysis* (Prentice Hall, Upper Saddle River, New Jersey, 2000), 2nd ed..

[2] D. Witthaut, F. Hellmann, J. Kurths, S. Kettemann, H. Meyer-Ortmanns, and M. Timme, Collective nonlinear dynamics and self-organization in decentralized power grids, Rev. Mod. Phys. **94**, 015005 (2022).

[3] M. Rohden, A. Sorge, M. Timme, and D. Witthaut, Self-organized synchronization in decentralized power grids, Phys. Rev. Lett. **109**, 064101 (2012).

[4] F. A. Rodrigues, T. K. D. Peron, P. Ji, and J. Kurths, The Kuramoto model in complex networks, Phys. Rep. **610**, 1 (2016).

[5] S. Kettemann, Delocalization of disturbances and the stability of ac electricity grids, Phys. Rev. E **94**, 062311 (2016).

[6] H. Haehne, K. Schmietendorf, S. Tamrakar, J. Peinke, and S. Kettemann, Propagation of wind-power-induced fluctuations in power grids, Phys. Rev. E **99**, 050301 (2019).

[7] L. Pagnier and P. Jacquod, Inertia location and slow network modes determine disturbance propagation in large-scale power grids, PLoS ONE **14**, e0213550 (2019).

[8] L. A. Torres-Sánchez, G. T. Freitas de Abreu, and S. Kettemann, Analysis of the dynamics and topology dependencies of small perturbations in electric transmission grids, Phys. Rev. E **101**, 012313 (2020).

[9] M. Anvari, L. R. Gorjão, M. Timme, D. Witthaut, B. Schäfer, and H. Kantz, Stochastic properties of the frequency dynamics in real and synthetic power grids, Phys. Rev. Res. **2**, 013339 (2020).

[10] X. Zhang, D. Witthaut, and M. Timme, Topological determinants of perturbation spreading in networks, Phys. Rev. Lett. **125**, 218301 (2020).

[11] M. Tyloo, J. Hindes, and P. Jacquod, Finite-time correlations boost large voltage angle fluctuations in electric power grids, J. Phys.: Complexity **4**, 015006 (2023).

[12] J. Machowski, Z. Lubosny, J. W. Bialek, and J. R. Bumby, *Power System Dynamics: Stability and Control* (John Wiley, Hoboken, New Jersey, 2020), 3rd ed.

[13] G. Rogers, *Power System Oscillations* (Springer Science & Business Media, New York, USA, 2012).

[14] V. Venkatasubramanian and Y. Li, in *Bulk Power System Dynamics and Control—VI* (Cortina d'Ampezzo, Italy, 2004), p. 685.

[15] European Commission. Joint Research Centre, *CO2 Emissions of All World Countries: JRC/IEA/PBL 2022 Report* (Publications Office, Luxembourg, Luxembourg, 2022).

[16] K. Creighton, M. McClure, R. Skillen, and A. Rogers, in *Proceedings of the 12th International Workshop on Large-scale Integration of Wind Power into Power Systems as well as on Transmission Networks for Offshore Wind Power Plants* (Energynautics GmbH, Germany, 2013), p. 6.

[17] F. Paganini and E. Mallada, in *2017 55th Annual Allerton Conference on Communication, Control, and Computing (Allerton)* (IEEE, Monticello, IL, USA, 2017), p. 324.

[18] T. Kërçi, M. Hurtado, M. Gjergji, S. Tweed, E. Kennedy, and F. Milano, in *2023 IEEE Power & Energy Society General Meeting (PESGM)* (IEEE, Orlando, FL, USA, 2023), p. 1.

[19] F. Milano, F. Dörfler, G. Hug, D. J. Hill, and G. Verbič, in *2018 Power Systems Computation Conference (PSCC)* (IEEE, Dublin, Ireland, 2018), p. 1.

[20] J. Driesen and K. Visscher, in *2008 IEEE Power and Energy Society General Meeting – Conversion and Delivery of Electrical Energy in the 21st Century* (IEEE, Pittsburgh, PA, USA, 2008), p. 1.

[21] Q.-C. Zhong and G. Weiss, Synchronverters: Inverters that mimic synchronous generators, IEEE Trans. Ind. Electron. **58**, 1259 (2011).

[22] S. D'Arco and J. A. Suul, in *2013 IEEE Grenoble Conference* (IEEE, Grenoble, France, 2013), p. 1.

[23] W. Sang, W. Guo, S. Dai, C. Tian, S. Yu, and Y. Teng, Virtual synchronous generator, a comprehensive overview, Energies **15**, 6148 (2022).

[24] N. Soni, S. Doolla, and M. C. Chandorkar, Improvement of transient response in microgrids using virtual inertia, IEEE Trans. Power Delivery **28**, 1830 (2013).

[25] M. A. Torres L., L. A. C. Lopes, L. A. Morán T., and J. R. Espinoza C., Self-tuning virtual synchronous machine: A control strategy for energy storage systems to support dynamic frequency control, IEEE Trans. Energy Convers. **29**, 833 (2014).

[26] D. Li, Q. Zhu, S. Lin, and X. Y. Bian, A self-adaptive inertia and damping combination control of VSG to support frequency stability, IEEE Trans. Energy Convers. **32**, 397 (2017).

[27] J. Alipoor, Y. Miura, and T. Ise, Power system stabilization using virtual synchronous generator with alternating moment of inertia, IEEE J. Emerg. Sel. Top. Power. Electron. **3**, 451 (2015).

[28] F. Wang, L. Zhang, X. Feng, and H. Guo, An adaptive control strategy for virtual synchronous generator, IEEE Trans. Ind. Appl. **54**, 5124 (2018).

[29] A. Kasis, S. Timotheou, and M. Polycarpou, in *2021 60th IEEE Conference on Decision and Control (CDC)* (IEEE, Austin, TX, USA, 2021), p. 2788.

[30] A. Kasis, S. Timotheou, and M. Polycarpou, On the stability properties of power networks with time-varying inertia, ArXiv:2301.09202.

[31] Y. Liu and C. Shen, Equivalent inertia provided by droop control of fast frequency regulation resources, ArXiv:2212.00685.

[32] A. Bergen and D. Hill, A structure preserving model for power system stability analysis, IEEE Trans. Power Apparatus Syst. **PAS-100,** 25 (1981).

[33] See the Supplemental Material at http://link.aps.org/supplemental/10.1103/PRXEnergy.3.033003 for an intuitive example and additional data.

[34] C. Grigg, P. Wong, P. Albrecht, R. Allan, M. Bhavaraju, R. Billinton, Q. Chen, C. Fong, S. Haddad, S. Kuruganty, W. Li, R. Mukerji, D. Patton, N. Rau, D. Reppen, A. Schneider, M. Shahidehpour, and C. Singh, The IEEE reliability test system—1996. A report prepared by the Reliability Test System Task Force of the Application of Probability Methods Subcommittee, IEEE Trans. Power Syst. **14,** 1010 (1999).

[35] M. Tyloo, L. Pagnier, and P. Jacquod, The key player problem in complex oscillator networks and electric power

grids: Resistance centralities identify local vulnerabilities, Sci. Adv. **5,** eaaw8359 (2019).

[36] D. Klein and M. Randić, Resistance distance, J. Math. Chem. **12,** 81 (1993).

[37] L. Pagnier and P. Jacquod, Optimal placement of inertia and primary control: A matrix perturbation theory approach, IEEE Access **7,** 145889 (2019).

[38] B. K. Poolla, S. Bolognani, and F. Dörfler, Optimal placement of virtual inertia in power grids, IEEE Trans. Automat. Contr. **62,** 6209 (2017).

[39] J. Fritzsch and P. Jacquod, Long wavelength coherency in well connected electric power networks, IEEE Access **10,** 19986 (2022).

[40] J. W. Simpson-Porco, F. Dörfler, and F. Bullo, Droop-controlled inverters are Kuramoto oscillators, IFAC Proc. Vol. **45,** 264 (2012).